SOFT ROBOTICS
Volume 00, Number 00, 2020

DOI: 10.1089/soro.2019.0053

SoRo
Soft Robotics

Lightweight Highly Tunable Jamming-Based Composites

Yashraj S. Narang,[1,2] Buse Aktaş,[1] Sarah Ornellas,[3] Joost J. Vlassak,[1] and Robert D. Howe[1,4]

Abstract

Tunable-impedance mechanisms can improve the adaptivity, robustness, and efficiency of a vast array of engineering systems and soft robots. In this study, we introduce a tunable-stiffness mechanism called a ''sandwich jamming structure,'' which fuses the exceptional stiffness range of state-of-the-art laminar jamming structures (also known as layer jamming structures) with the high stiffness-to-mass ratios of classical sandwich composites. We experimentally develop sandwich jamming structures with performance-to-mass ratios that are far greater than laminar jamming structures (e.g., a 550-fold increase in stiffness-to-mass ratio), while simultaneously achieving tunable behavior that standard sandwich composites inherently cannot achieve (e.g., a rapid and reversible 1800-fold increase in stiffness). Through theoretical and computational models, we then show that these ratios can be augmented by several orders of magnitude further, and we provide an optimization routine that allows designers to build the best possible sandwich jamming structures given arbitrary mass, volume, and material constraints. Finally, we demonstrate the utility of sandwich jamming structures by integrating them into a wearable soft robot (i.e., a tunable-stiffness wrist orthosis) that has negligible impact on the user in the off state, but can reduce muscle activation by an average of 41% in the on state. Through these theoretical and experimental investigations, we show that sandwich jamming structures are a lightweight highly tunable mechanism that can markedly extend the performance limits of existing structures and devices.

Keywords: tunable stiffness, jamming, composite, sandwich, orthosis

Introduction

Tunable-impedance mechanisms (e.g., tunable-stiffness materials and structures) can improve the adaptivity, safety, robustness, and energy efficiency of a diverse array of engineering systems.[1] One class of tunable-impedance mechanisms is jamming structures. In comparison with other such mechanisms, these structures have high impedance range, impedance resolution, conformability in the inactivated state, and activation speed, as well as low cost and difficulty of fabrication.[2–4] Jamming structures have been effectively used in robotic manipulators,[4–7] haptic interfaces,[8–12] medical devices,[2,13–15] and locomotion and aerospace structures.[16–18]

Research on jamming mechanisms has primarily focused on two types of structures: granular jamming structures and laminar jamming (a.k.a., ''layer jamming'') structures. Granular jamming structures typically consist of collections of particles (e.g., coffee grounds) enclosed in an airtight envelope. When vacuum is applied to the envelope, kinematic and frictional coupling increase, augmenting the stiffness and damping of the structure. The jammed structures are highly resistant to compression and shear loads, but inherently fragile in tension and bending due to particle separation and dislocations.[14,15,19]

Similarly, laminar jamming structures typically consist of flexible layers, usually of a single type of material (e.g., strips of fabric), enclosed in an airtight envelope. When vacuum is applied, frictional coupling increases, again augmenting the stiffness and damping of the structure. Laminar jamming structures are exceptionally resistant to bending[4]; furthermore, they have an inherently thin lightweight form factor. These properties make laminar jamming structures particularly suitable for integration into tunable soft robotic manipulators and wearable devices, which often require high maximum bending stiffness and low physical profile, both relative to mass.

[1]Paulson School of Engineering and Applied Sciences, Harvard University, Cambridge, Massachusetts, USA.
[2]NVIDIA Corporation, Seattle, Washington, USA.
[3]Department of Biomedical Engineering, School of Engineering and Applied Science, Yale University, New Haven, Connecticut, USA.
[4]Hansjörg Wyss Institute for Biologically Inspired Engineering at Harvard University, Boston, Massachusetts, USA.

There are numerous applications in which mass is critical; these applications demand laminar jamming structures with even higher performance-to-mass ratios. For example, in assistive devices, researchers have used laminar jamming structures to selectively immobilize injured joints.[20,21] However, as documented in previous study,[4,8] laminar jamming structures begin to yield (i.e., exhibit a decreased bending stiffness) after a critical transverse load is exceeded and adjacent layers start to slide. To prevent yielding, the structures can be thickened, but it is well established that adding mass to the body increases metabolic energy expenditure.[22,23] As a second example, in quadcopter design, laminar jamming structures have been used to construct landing gear with a tunable impact response.[18] However, the lift-to-drag ratio of aerial vehicles decreases monotonically and dramatically with higher mass.[24] As these cases demonstrate, minimizing the mass of laminar jamming structures is often essential for practical use.

To improve the performance-to-mass of laminar jamming structures, we introduce the concept of *sandwich jamming structures*. Sandwich jamming structures are inspired by standard sandwich panels, which comprise one of the fundamental categories of modern composites. Sandwich panels consist of thin stiff faces (made of materials such as aluminum) permanently bonded to a thick low-density core (made of materials such as polyethylene). Owing to the geometric separation of the stiff faces (analogous to an I-beam) and the shear and buckling resistance of the core, the combination has outstanding stiffness-to-mass properties. These structures first came into widespread use during the initial development of military aircraft, and they have since been applied to industries as diverse as construction, automobile engineering, and spacecraft design.[25]

The *sandwich jamming structures* presented in this study take the form of sandwich panels, as they consist of stiff face material and compliant core material. However, similar to laminar jamming structures, the faces and core are divided into numerous unbonded laminae, all enclosed within an airtight envelope (Fig. 1A). When no vacuum is applied, the structure is highly compliant; however, when vacuum is applied, frictional coupling dramatically increases between the laminae, and the structure effectively transforms into a sandwich panel. As we show, sandwich jamming structures have far higher performance-to-mass ratios than laminar jamming structures—specifically, higher maximum stiffness, stiffness range (i.e., the ratio of the jammed to unjammed stiffness), and yield force, all with respect to mass. Such performance also greatly exceeds that of other tunable sandwich structures in the literature.[26–30]

Furthermore, sandwich jamming structures are far more mechanically versatile than standard sandwich panels. They can adapt their stiffness and damping to the environment (e.g., as aerodynamic and hydrodynamic control surfaces), can be molded to an arbitrary initial shape (e.g., when conforming to the body), and can recover their undeformed configuration after yielding (e.g., after impacts). In summary, sandwich jamming structures have far higher performance-to-mass ratios than laminar jamming structures, as well as far greater versatility than sandwich panels.

Objective

In this study, we first experimentally demonstrate that sandwich jamming structures have far higher performance-to-mass ratios than laminar jamming analogues. We then present detailed theoretical and finite-element models that parametrically describe how and to what extent laminar jamming structures can be improved by converting them to a sandwich jamming architecture. Next, we provide an optimization tool that allows designers to input an arbitrary set of materials and mass–volume constraints and then identify the highest performance sandwich jamming structure that can be constructed within those bounds. Finally, we demonstrate the utility of sandwich jamming structures by integrating them into a wearable soft robot (i.e., a lightweight conformable tunable-stiffness wrist orthosis) that can markedly reduce muscle activation when turned on and preserve natural range of motion when turned off.

Through this study, we contribute the concept of tunable jamming-based sandwich structures, which, in general, also comprise one of the first examples of jamming-based composites. Furthermore, we impart designers with an analysis and simulation toolkit that allows them to relate the design parameters of sandwich jamming structures (e.g., the number of layers in the face and core) to performance specifications (e.g., stiffness range), as well as optimize the performance of

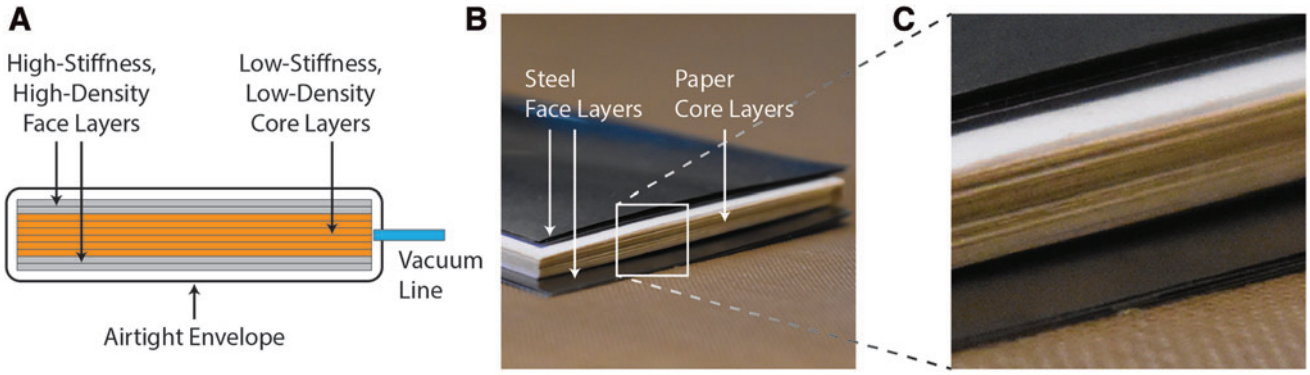

FIG. 1. Concept and physical prototype of sandwich jamming structures. **(A)** Conceptual diagram of a sandwich jamming structure. Face layers and core layers are enclosed in an airtight envelope connected to a vacuum line. When vacuum is applied, the structure exhibits a dramatic change in mechanical properties. **(B, C)** Physical prototype of a steel-paper sandwich jamming structure. The layers within the airtight envelope are depicted. Color images are available online.

the structures. Overall, we demonstrate that sandwich jamming structures can advance the state of the art in tunable-stiffness mechanisms, and we provide the means to further their development within soft robotics and other fields.

Materials and Methods

The following is a highly abridged description of the materials and methods used in this study. For complete detail, please see Supplementary Data.

Experimental proof of concept

To validate the concept of sandwich jamming structures, prototypes were constructed and experimentally characterized. The primary goal of the investigation was to determine whether sandwich jamming structures could achieve higher performance-to-mass ratios than laminar jamming structures. As described earlier, each sandwich structure consisted of faces composed of unbonded stiff laminae and a core composed of unbonded compliant lightweight laminae, all within an airtight envelope. When no vacuum is applied the structure is highly compliant, and when vacuum is applied the structure effectively transforms into a standard sandwich panel. Accordingly, the heuristics of modern sandwich panel construction were followed.[25,31] Specifically, all sandwich jamming structures were constructed such that the small-deformation stress–strain modulus of the face material was at least an order of magnitude greater than that of the core material, and the total thickness of the core was at least an order of magnitude greater than the total thickness of the faces.

Paper, polyurethane (PU) foam, low-density polyethylene (LDPE), and low-carbon steel were chosen as candidate materials for the face and core, as the materials were low cost, exhibited negligible electrostatic attraction, and could be effectively cut using standard laboratory equipment. Specifically, sandwich jamming structures were fabricated with the following material configurations: (1) low-carbon steel face laminae and paper core laminae (Fig. 1B, C), (2) low-carbon steel face laminae and LDPE core laminae, and (3) paper face laminae and PU foam core laminae. For each material configuration, structures were built using various numbers of core layers.

Multiple samples were fabricated for each material configuration. For each sample, individual laminae were cut from raw stock using a laser cutter (VLS4.60; Universal Laser Systems, Inc., Scottsdale, AZ), metal shears, or razor blades. The laminae were stacked and placed inside an airtight thermoplastic elastomer envelope (Fibre Glast Developments Corp., Brookville, OH). The envelope was sealed using an impulse sealer (AIE-450FD; American International Electric, Inc., City of Industry, CA), and a plastic tube was inserted as a vacuum line.

Each sample was placed onto a universal materials testing device (Instron 5566; Illinois Tool Works, Norwood, MA), and the desired vacuum pressure was applied or removed using a manual vacuum regulator to activate or deactivate jamming, respectively. The sample was then loaded in three-point bending (Fig. 2A), and the force versus deflection relationships were measured during loading and unloading.

Three performance metrics were extracted from the experimental data: jammed stiffness, stiffness range (i.e., the ratio of jammed to unjammed stiffnesses), and yield force (i.e., the transverse force at which the jammed stiffness tends to decrease due to sliding between the layers), all divided by mass. Using previously reported theory,[4] the same performance metrics were calculated for laminar jamming structures consisting of just the face laminae. The performance metrics of the sandwich jamming structures were then divided by the corresponding values for the laminar jamming structures (e.g., the performance metrics for a sandwich jamming structure consisting of 2 layers of steel, 20 layers of paper, and 2 layers of steel were divided by the corresponding values for a laminar jamming structure consisting of 4 layers of steel). These quotients comprised ''improvement ratios'' that described how much higher the performance metrics of the sandwich jamming structures were in comparison with corresponding laminar jamming structures.

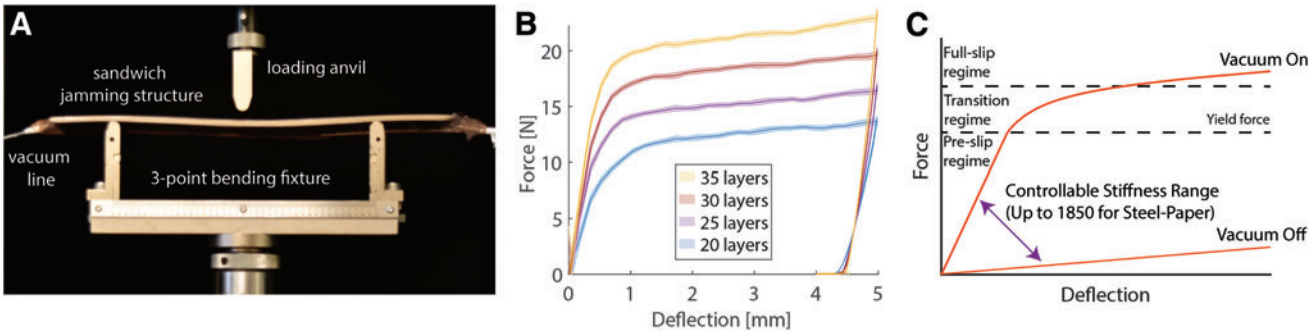

FIG. 2. Fundamental behavior of sandwich jamming structures. **(A)** Experimental setup to measure force versus deflection curves of sandwich jamming structures in three-point bending. **(B)** Force versus deflection curves of steel-paper sandwich jamming structures at 71 kPa vacuum pressure during both loading and unloading. Curves are shown for different numbers of core layers. Each curve is a mean curve from 2 samples and 10 trials. *Shaded error bars* denote standard error. **(C)** Conceptualized force versus deflection behavior during loading. As with standard laminar jamming structures,[4] when vacuum is applied, the force versus deflection curves of sandwich jamming structures during loading consist of a high-stiffness regime (preslip), a yield force, a transition regime, and a low-stiffness regime (full slip). (For simplicity, the unloading curve is not drawn.) When vacuum is not applied, the force versus deflection curves simply consist of a single low-stiffness regime. The difference in the slopes between the vacuum on and vacuum off states defines the stiffness range, which was measured to be up to 1850 for the steel-paper sandwich jamming structures in this study. Color images are available online.

Theoretical modeling

Following the experimental proof of concept, a general question was considered: given a set of laminar jamming structures (e.g., ones that have been selected for a specific application), by what factor can their performance metrics be improved by converting them to sandwich jamming structures? In equivalent terms, what are the best-case experimental ''improvement ratios''? To answer this question, theoretical expressions for the improvement ratios were derived. The expressions were intended to articulate exactly how these ratios scale with critical design parameters (e.g., elastic moduli of the faces), providing the basis for subsequent design optimization.

The most basic strategy to convert a laminar jamming structure into a sandwich jamming structure is to simply add core layers. However, in the real world, this strategy may be infeasible due to strict mass and volume constraints. For generality, all modeling was repeated for three different constraints that are relevant when converting laminar jamming structures into sandwich jamming structures. These constraints are as follows:

1. An ''equal-material'' constraint, in which maintaining cost is the primary concern. *All* the sheets of the laminar jamming structure are used as face laminae for the sandwich jamming structure, and core laminae (which are relatively compliant and typically far less expensive) can be added arbitrarily (Fig. 3A). Note that this strategy is the ''most basic strategy'' just mentioned.
2. An ''equal-mass'' constraint, in which preserving mass is the primary concern. A *subset* of the sheets of the laminar jamming structure are used as face laminae for the sandwich jamming structure, and core laminae can be added with the constraint that the total *mass* of the sandwich must be equal to the mass of the laminar jamming structure (Supplementary Figure S1A).
3. An ''equal-volume'' constraint, in which preserving volume is the primary concern. A *subset* of the sheets of the laminar jamming structure are used as face laminae for the sandwich jamming structure, and core laminae can be added with the constraint that the total *volume* of the sandwich must be equal to the volume of the laminar jamming structure (Supplementary Fig. S2A).

For sake of brevity, this section only provides formulae for improvement ratios given an ''equal-material'' constraint; a detailed consideration of the equal-mass and equal-volume constraints is included in Theoretical Modeling section of Supplementary Data.

To determine how the performance-to-mass metrics of standard laminar jamming structures could be improved by converting them to a sandwich architecture (with an equal-material constraint), the theoretical performance-to-mass of

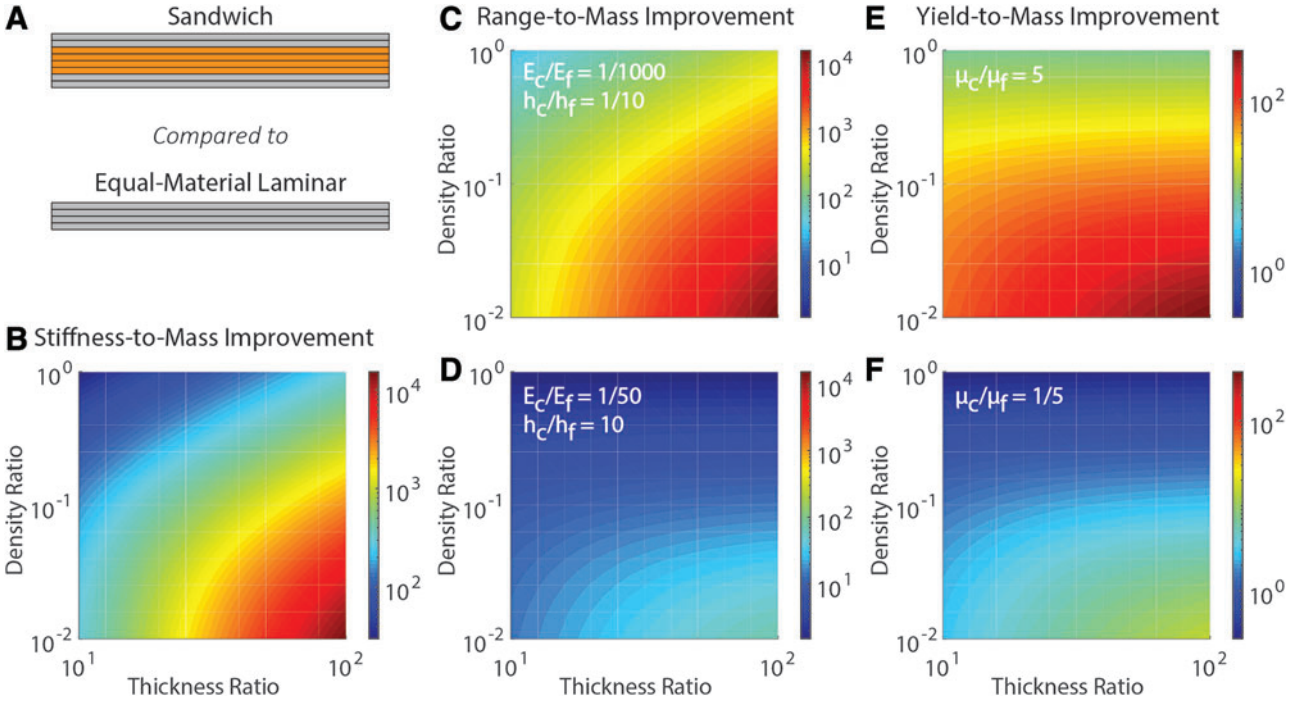

FIG. 3. Contour maps of improvement ratios for a sandwich jamming structure compared with an equal-material laminar jamming structure. **(A)** Conceptual diagrams of the compared jamming structures. **(B–F)** Contour maps of improvement ratios. Each plot illustrates performance improvement as a function of density ratio ($\frac{\rho_c}{\rho_f}$) and total thickness ratio ($\frac{c}{f}$). Range-to-mass improvement is also a function of the product of the elastic modulus ratio and the square of the layer thickness ratio ($\frac{E_c}{E_f}(\frac{h_c}{h_f})^2$), and yield-to-mass improvement is also a function of the coefficient of friction ratio ($\frac{\mu_c}{\mu_f}$). Thus, two plots are provided for each of these performance metrics to show variation with these additional parameters. Design parameters are varied over a range representative of real-world limits. Note that both stiffness-to-mass and range-to-mass can be improved by four orders of magnitude, and yield-to-mass can be improved by two orders of magnitude. Color images are available online.

both types of structures was first calculated. As in the experimental proof of concept, three performance-to-mass metrics were computed: (1) maximum bending stiffness, (2) bending stiffness range, and (3) yield force, all divided by mass. Ratios were then computed of the performance-to-mass metrics of the sandwich jamming structure to the corresponding metrics of a standard laminar jamming structure. The ratios were expressed as functions of critical nondimensional design parameters.

For standard laminar jamming structures, the performance metrics were calculated using classical (i.e., Euler–Bernoulli) beam theory. An excellent discussion of classical beam theory is provided in Ref.[32], and a detailed description of how to apply the theory to laminar jamming structures is provided in Ref.[4]. For sandwich jamming structures, the performance metrics were calculated using sandwich beam theory, a well-established theory in structural mechanics used for predicting the load–deformation relationships of sandwich panels. Sandwich theory is based on Timoshenko beam theory, which itself extends classical theory to include the effects of shear deformations within beams. However, sandwich theory makes the additional assumptions that (1) the beam consists of two faces and a core, (2) the faces are much thinner than the core, and (3) the core is much more compliant than the faces. Excellent references on sandwich theory include Refs. [25,31,33,34] and the following paragraphs summarize key formulae that result from applying sandwich theory to sandwich jamming structures. Please note that step-by-step derivations are provided in Theoretical Modeling section of Supplementary Data.

From sandwich theory, the jammed stiffness of a sandwich jamming structure (i.e., a solid sandwich beam) is approximately $E_f b\frac{4c^2f+4cf^2+f^3}{16}$, where E_f is the elastic modulus of the face material; b is the width; and c and f are the total thickness of the core and face, respectively. From classical beam theory, the jammed stiffness of a laminar jamming structure (i.e., a solid standard beam) is $\frac{EbH^3}{12}$, where E is the elastic modulus of the layers and H is the total thickness. We used these expressions to algebraically derive the stiffness-to-mass improvement ratio, which is

$$\left(\frac{k_b}{m}\right)^* = \frac{12(\frac{c}{f})^2 + 12\frac{c}{f} + 3}{4(\frac{\rho_c}{\rho_f}\frac{c}{f} + 1)}, \tag{1}$$

where $(\frac{k_b}{m})^*$ is the dimensionless ratio of the bending-stiffness-to-mass of the sandwich jamming structure to that of the laminar jamming structure, $\frac{c}{f}$ is the ratio of the total thickness of the core to that of the faces, and $\frac{\rho_c}{\rho_f}$ is the ratio of the density of the core material to the density of the face material.

To calculate the range of a jamming structure, the unjammed stiffness must be computed as well. From classical beam theory, the unjammed stiffness of a sandwich jamming structure (i.e., a decoupled stack of solid sandwich beams) is $b\frac{E_c n_c h_c^3 + E_f n_f h_f^3}{12}$, where E_c is the elastic modulus of the core, n_c and n_f are the total number of layers in the core and faces, respectively, and h_c and h_f are the thickness of each core and face layer, respectively. The unjammed stiffness of a laminar jamming structure (i.e., a decoupled stack of solid standard beams) is $\frac{Ebnh^3}{12}$. We used these expressions to algebraically derive the range-to-mass improvement ratio, which is

$$\left(\frac{r}{m}\right)^* = \frac{12(\frac{c}{f})^2 + 12\frac{c}{f} + 3}{4(\frac{E_c}{E_f}(\frac{h_c}{h_f})^2\frac{c}{f} + 1)(\frac{\rho_c}{\rho_f}\frac{c}{f} + 1)}, \tag{2}$$

where $(\frac{r}{m})^*$ is the ratio of the range-to-mass of the sandwich jamming structure to that of the laminar jamming structure, and $\frac{E_c}{E_f}$ is the ratio of the elastic modulus of the core material to that of the face material.

Finally, to calculate the yield force of a jamming structure, the maximum induced shear stress must be equated with the maximum allowable shear stress (as limited by friction and pressure). For a sandwich jamming structure, we derived the yield force to be approximately $2bc\mu_c P$, where μ_c is the coefficient of friction of the core material and P is the vacuum pressure; for a laminar jamming structure, the yield force is $\frac{4}{3}bH\mu P$, where μ is the coefficient of friction of the layers.[4] We used these expressions to derive the yield-to-mass improvement ratio, which is

$$\left(\frac{F_{crit}}{m}\right)^* = \frac{3}{2}\frac{\mu_c}{\mu_f}\frac{\frac{c}{f}}{\frac{\rho_c}{\rho_f}\frac{c}{f} + 1}, \tag{3}$$

where $(\frac{F_{crit}}{m})^*$ is the ratio of the yield force of the sandwich jamming structure to that of the laminar jamming structure, and $\frac{\mu_c}{\mu_f}$ is the ratio of the coefficient of friction of the core material to that of the face material.

Validation of theoretical model

Finite element simulations were conducted to corroborate the predictions of the theoretical model. Simulations were generated and executed using commercial simulation software (Abaqus 2017; Dassault Systèmes, Vélizy-Villacoublay, France). Each layer was modeled as a two-dimensional body, and frictional contact was prescribed at the interfaces between adjacent layers. A uniform mesh of quadrilateral elements was used, with two elements across the thickness of each face layer. Vacuum pressure was applied, and the structures were loaded in three-point bending (Fig. 4A–C). A static implicit solver was selected, and large-deformation analysis and automatic time-stepping were enabled.

The simulations were executed for a range of design parameters that could be achieved with common laboratory materials (e.g., standard metals and plastics). Since the simulations were static rather than dynamic, inertia was negligible; thus, the density ratio was not varied, as it did not affect the output. All parameters used in the simulations are tabulated in Validation of Theoretical Model: Finite Element Analysis section of Supplementary Data.

From the simulations, force versus deflection curves were extracted. As with the experimental data, the stiffness, range, and yield forces were extracted from these curves.

Experimental tests were also conducted to evaluate the predictions of the theoretical model for a steel-paper sandwich jamming structure. The experimental procedure was nearly identical to that described earlier for testing of initial prototypes in Materials and Methods: Experimental Proof of Concept. Further details are provided in Validation of Theoretical Model: Experimental Comparison section of Supplementary Data, with illustrations in Supplementary Figure S3.

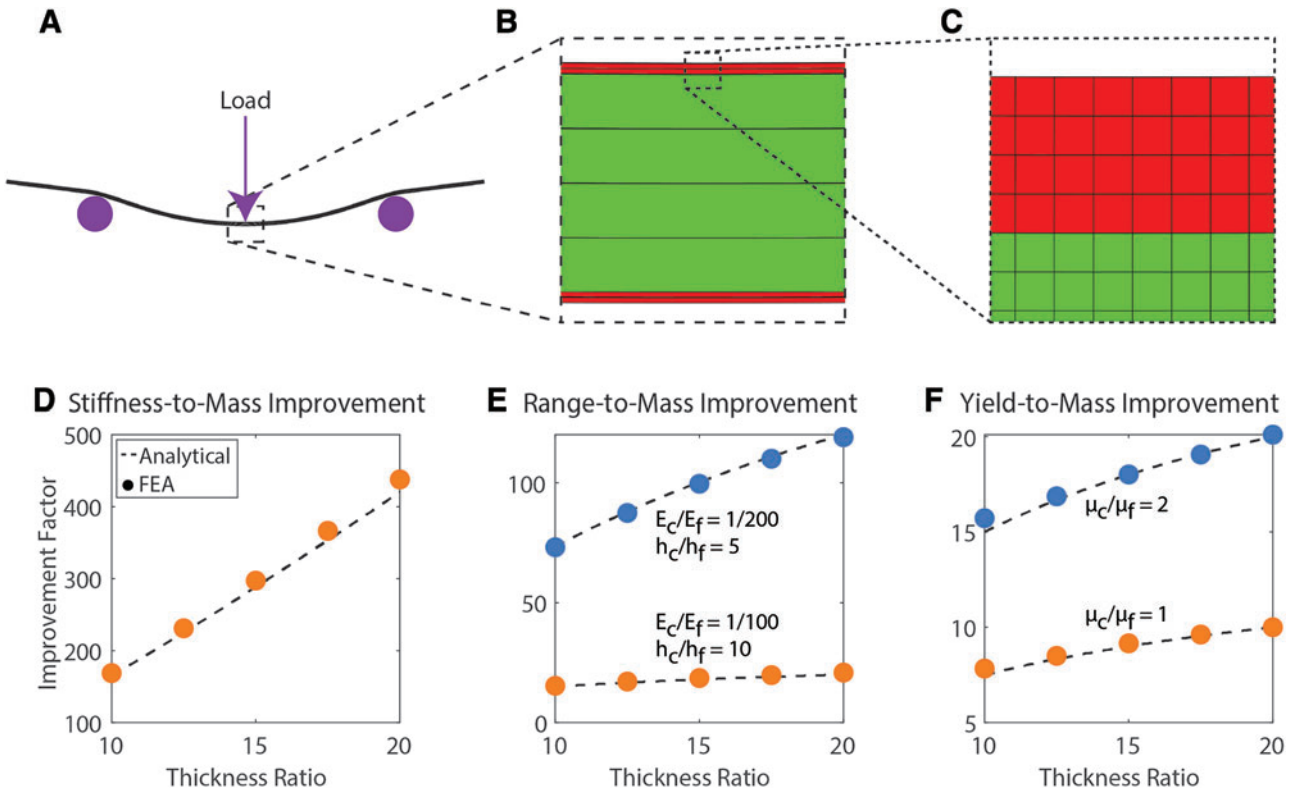

FIG. 4. Validation of theoretical model with FEA. (**A–C**) Schematic of finite element model, showing face layers, core layers, and mesh. (**D–F**) Comparison of theoretically predicted improvement ratios to finite element results. *Dashed lines* denote theoretical predictions, and *filled circles* denote finite element results. The theoretically predicted stiffness-to-mass, range-to-mass, and yield-to-mass improvement ratios were all closely corroborated by finite element values. The minimum coefficient of determination (R^2) between any theoretical and finite element data set was 0.992 for the yield-to-mass improvement ratios with $\frac{\mu_c}{\mu_f} = 2$. Full dimensional and material parameters for the finite element simulations are provided in Supplementary Table S1, and raw output is shown in Supplementary Figure S4. FEA, finite element analysis. Color images are available online.

Optimization

The preceding analysis and simulations determined exactly how and to what extent given laminar jamming structures can be improved by converting them to a sandwich architecture (i.e., by adding a core). However, for a designer who is building sandwich jamming structures from the ground up, it is also important to identify the sandwich jamming structure with the best-possible performance-to-mass ratios, rather than the best-possible improvement ratio for a given laminar jamming structure. Furthermore, the designer may be constrained by a maximum mass, a maximum volume, and a particular set of real-world materials.

This problem is theoretically challenging for two major reasons. First, although performance improvement ratios (e.g., stiffness-to-mass improvement ratio) are dimensionless and can be expressed as a function of a small number of nondimensional parameters (e.g., $\frac{\rho_c}{\rho_f}$), performance metrics themselves (e.g., stiffness-to-mass ratio) are dimensional and cannot be analogously simplified (e.g., the absolute magnitudes of both ρ_c and ρ_f may be critical). Thus, maximizing performance requires investigation of a much larger parameter space, which becomes difficult to plot and intuitively understand. Second, real-world materials do not allow arbitrary variations of material parameters (e.g., ρ, E, μ) with respect to one another; as a result, many discrete constraints must be imposed.

The preceding problem was effectively addressed through numerical optimization using mathematical analysis software (MATLAB 2018a; MathWorks, Natick, MA). A software routine was written that first allows designers to input an arbitrary set of available materials, as well as any mass, volume, and layer thickness constraints relevant to their application. Next, the routine cycles through each possible pair of core and face materials and determines which pairs satisfy the assumptions of sandwich theory (i.e., $E_c << E_f$). For each pair of materials, the routine optimizes the geometry of the face, core, and individual laminae using a constrained nonlinear optimization algorithm (*fmincon*) to maximize the stiffness-to-mass, range-to-mass, and yield-to-mass ratios of the structure. The constraints are mass, volume, and layer thickness constraints specified by the user, and the optimized parameters are geometric variables. The cost functions are simply the reciprocals of the performance-to-mass expressions for sandwich jamming structures derived in Theoretical Modeling section of Supplementary Data. Finally, for each of these performance metrics, the optimization routine determines the best-performing structure. A flowchart of the routine is shown in Supplementary Figure S6.

A case study was used to illustrate the results of the routine. Four materials were input into the software routine (i.e., paper, LDPE, PU foam, and low-carbon steel), along with their material properties and minimum available

thicknesses (Supplementary Table S2). Arbitrary mass and volume constraints were applied.

Design example

Sandwich jamming structures may be useful in a range of applications, including assistive devices, vehicles, and deployable structures. We explored the first category by constructing a wrist orthosis with a sandwich jamming structure as a tunable-stiffness element. For patients with wrist injuries, a tunable-stiffness orthosis may reduce muscle activation during static weight-bearing tasks (e.g., carrying grocery bags), but enable flexibility during nonstrenuous dynamic tasks (e.g., driving). A sandwich jamming structure presents a highly compelling tunable-stiffness structure for this application, as it not only has high stiffness-to-mass, range-to-mass, and yield-to-mass ratios, but is also thin, conformable, and rapidly activated. Thus, we built a sandwich-jamming wrist orthosis that was intended to facilitate isometric hold tasks when the structure was jammed, but allow full range of motion when unjammed.

The orthosis consisted of two separate nonslip fabric sleeves for both the hand and the arm. A sandwich jamming structure was attached to the palmar side of the hand through a hook-and-loop (i.e., Velcro) strap and was allowed to slide freely along the long axis of the arm within a low-friction pocket sewn on the proximal sleeve (Fig. 6A). Electromyography (EMG) electrodes were placed on the skin above the flexor carpi ulnaris muscle to measure muscle activation (Fig. 6B). This muscle was selected for two major reasons: (1) it is one of the dominant wrist flexor muscles, and (2) it is located superficially within the arm, facilitating placement of EMG electrodes. To place the electrodes, subjects were asked to flex their wrists, and the middle of the muscle belly was identified through palpation. Electrodes were placed directly above this location.

The optimization software routine was used to determine the materials and geometry of a high-performance sandwich jamming structure that satisfied specific mass and volume constraints; the sandwich jamming structure consisted of 6 layers of low-carbon steel, 30 layers of paper, and 6 layers of steel.

To evaluate the performance of the brace during weight-bearing activities, an isometric hold task was conducted on nine human subjects (Fig. 6B, C). The orthosis was fastened onto each subject, and EMG electrodes were located above the wrist flexor muscles. Each subject was requested to bend their elbow to 90° and freely rest it on a flat surface. A weight was suspended from their hand, and the subject was requested to keep their wrist flat with minimal effort. Muscle activation was recorded. The test was conducted with (1) no orthosis, (2) the sandwich jamming brace in the inactive (i.e., unjammed) state, and (3) the brace in the active (i.e., jammed) state. For each subject, the EMG signal was normalized by the average EMG signal during a maximum voluntary contraction.

To evaluate the flexibility of the brace during nonweight-bearing activities, a range-of-motion test was also conducted (Fig. 6D). During these tests, subjects were asked to flex and extend their wrists to the maximum angle that they still perceived as comfortable; the difference in angles was measured. The test was executed three times each for the no-brace and inactive conditions. A paired samples *t*-test was conducted.

Results

Experimental proof of concept

Figure 2B shows force deflection curves for a high-performing material configuration that consisted of steel face layers and paper core layers. (Supplementary Fig. S6 shows analogous curves for an additional material configuration.) Figure 2C illustrates the general behavior of such structures.

For the steel-paper configuration, the jammed stiffness increased by up to a factor of 1850; furthermore, the maximum stiffness-to-mass, range-to-mass, and yield-to-mass improvement ratios were 560, 86, and 27, respectively. (Supplementary Table S3 provides the improvement ratios for additional material configurations.) The results demonstrated that by converting laminar jamming structures to sandwich jamming structures, performance improvements of one to two orders of magnitude could be readily achieved, motivating subsequent analysis and optimization.

Theoretical modeling

Figure 3B–F provides contour maps that illustrate the functional dependence of the three improvement ratios (i.e., stiffness-to-mass improvement, range-to-mass improvement, and yield-to-mass improvement) on the nondimensional design parameters (i.e., density ratio and thickness ratio) while imposing an equal-material constraint. As shown in the plots, the improvement ratios are nonlinear functions of the design parameters, with notable covariance. By converting a laminar jamming structure to a sandwich jamming structure, stiffness-to-mass and range-to-mass can both be readily improved by more than four orders of magnitude, and yield-to-mass can be improved by more than two orders of magnitude. These improvements can be achieved by maximizing the total thickness ratio and friction ratio, and minimizing the density ratio, elastic modulus ratio, and layer thickness ratio.

Validation of theoretical model

Figure 4D–F compares theoretical predictions and finite element results. As illustrated, finite element simulations corroborated theoretical predictions with exceptional fidelity. In fact, the *minimum* coefficient of determination (R^2) between theoretical predictions and finite element results was >0.99, indicating that the theoretical model exhibited excellent accuracy relative to a sophisticated computational reference.

Experimental results for a steel-paper sandwich jamming structure also closely supported theoretical predictions. In particular, for lower numbers of core layers (i.e., 20 and 25 layers), theoretically predicted improvement ratios deviated from experimental results by not >13%. Numerical results for all numbers of layers and corresponding analyses are provided in Validation of Theoretical Model: Experimental Comparison section of Supplementary Data.

Optimization

The routine identified five material pairs (i.e., steel-paper, steel-LDPE, steel-foam, paper-foam, and LDPE-foam) that satisfied the assumptions of sandwich theory and recommended construction guidelines (i.e., $E_c >> E_f$).[25,31] For the range-to-mass ratio, Table 1 lists the best-performing sandwich structures for each material configuration, as well as

Table 1. Results from the Optimization Case Study for the Range-to-Mass Ratio

	Optimized parameter				
Material configuration	n_c	$h_c[m]$	n_f	$h_f[m]$	*Range-to-mass* $[\frac{1}{kg}]$
Steel-paper	66	6.7e-3	2	5.0e-4	4.6e4
Steel-LDPE	63	6.4e-3	2	5.0e-4	4.5e4
Steel-foam	8	7.0e-3	2	5.0e-4	6.8e4
Paper-foam	8	6.8e-3	6	6.8e-4	5.2e5
LDPE-foam	8	6.8e-3	6	6.8e-4	8.0e4

Arbitrary mass constraints (total mass $\leq 47g$) and volume constraints (width $= 50\,mm$, length $= 100\,mm$, and total height $\leq 7.5\,mm$) were applied.
LDPE, low-density polyethylene.

their corresponding geometric properties. (Supplementary Tables S4 and S5 provide analogous data for the stiffness-to-mass and yield-to-mass ratios, respectively.)

In practical scenarios, mass and volume constraints may change frequently during prototyping. To provide designers with intuition about how a change of constraints can influence optimal geometries, the software routine can also generate contour maps that show how performance metrics vary with geometry, with constraints directly illustrated on the maps. Figure 5 shows an example of these contour maps for a sandwich jamming structure consisting of steel face layers and paper core layers. To use these maps, the designer first chooses mass and/or volume constraints on the map. The designer then looks for the highest value of the performance metric (from the color bar) that lies to the left of the constraint lines. The optimal geometry is given by the x- and y-coordinates of this value, which denote the number of core and face layers, respectively. This process can be easily repeated for another set of mass and volume constraints as desired.

Design examples

For the isometric hold task, Figure 6E shows muscle activation profiles (i.e., EMG signals) across the three evaluated conditions (i.e., no brace, inactive brace, and active brace) for a single representative subject, and Figure 6F depicts the average signal magnitudes across all nine subjects. Paired t-tests indicated that the active and inactive conditions exhibited a statistically significant difference ($p = 0.006$), demonstrating that the brace reduced musculoskeletal demand when activated; specifically, the average EMG signal magnitudes were reduced by a mean of 40.7% (standard error = 9.9%). In contrast, the inactive and no-brace conditions did not exhibit a statistically significant difference ($p = 0.70$), indicating that wearing the inactive brace did not affect baseline musculoskeletal demand.

For the range-of-motion test (Fig. 6D), the two evaluated conditions (i.e., no brace and inactive brace) exhibited a statistically significant difference ($p = 0.014$); however, subjects in the inactive state achieved an average of 94% of the angular range of motion that they achieved in the no-brace state (standard error = 1.8%). Thus, although range of motion was affected, it was essentially preserved.

Discussion

This study introduced the concept of tunable jamming-based sandwich structures through experiments, models, and demonstrations. We first experimentally showed that simple sandwich jamming structures can achieve notably higher performance than laminar jamming structures. We then presented a theoretical model that describes how the performance-to-mass of laminar jamming structures can be improved by converting to a sandwich jamming architecture. This theoretical model explicitly relates critical design parameters (e.g., core-to-face thickness ratios) to performance metrics and was corroborated by finite-element simulations and experiments. Next, we provided an optimization tool that can identify the best-possible sandwich jamming configuration given an arbitrary set of materials and mass–volume constraints. Finally, we demonstrated the utility of sandwich jamming structures by showing that a sandwich-jamming wrist orthosis can reduce muscle activation in isometric hold tasks when jammed, while allowing significant range of motion when unjammed. Collectively, our models, experiments, and demonstrations provide a full theoretical and empirical description of a novel structure that advances the state of the art in tunable-stiffness mechanisms.

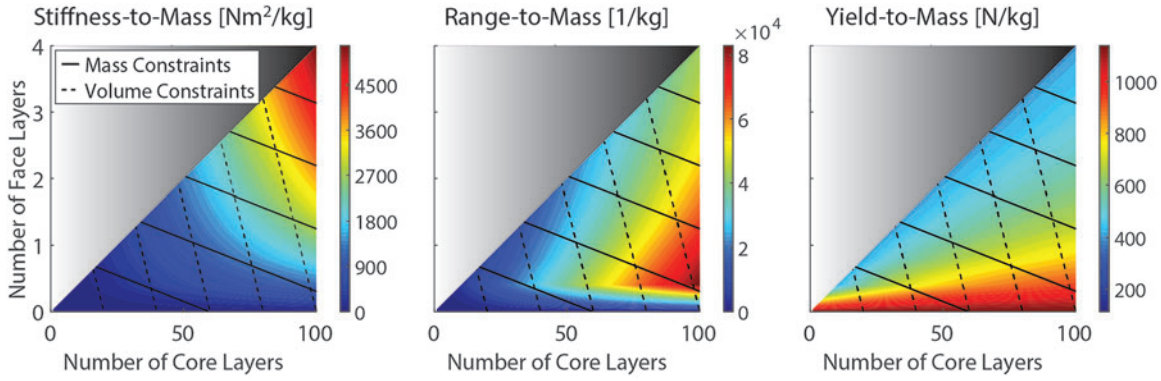

FIG. 5. Contour maps for optimization of steel-paper sandwich structures. The plots illustrate the variation of optimal performance values and corresponding geometries (i.e., number of core and face layers) with applied constraints (i.e., maximum mass and/or volume). The mass and volume constraints are shown in *solid* and *dashed lines*, respectively, on each graph; from left to right, the mass constraints are $\{24, 48, 72, 96, 120\}g$, and the volume constraints are a maximum height of $\{2, 4, 6, 8, 10\}mm$. *Grayscale regions* do not satisfy a fundamental assumption of sandwich theory (i.e., $c >> f$), where c and f are the total thickness of the core and both faces, respectively. Color images are available online.

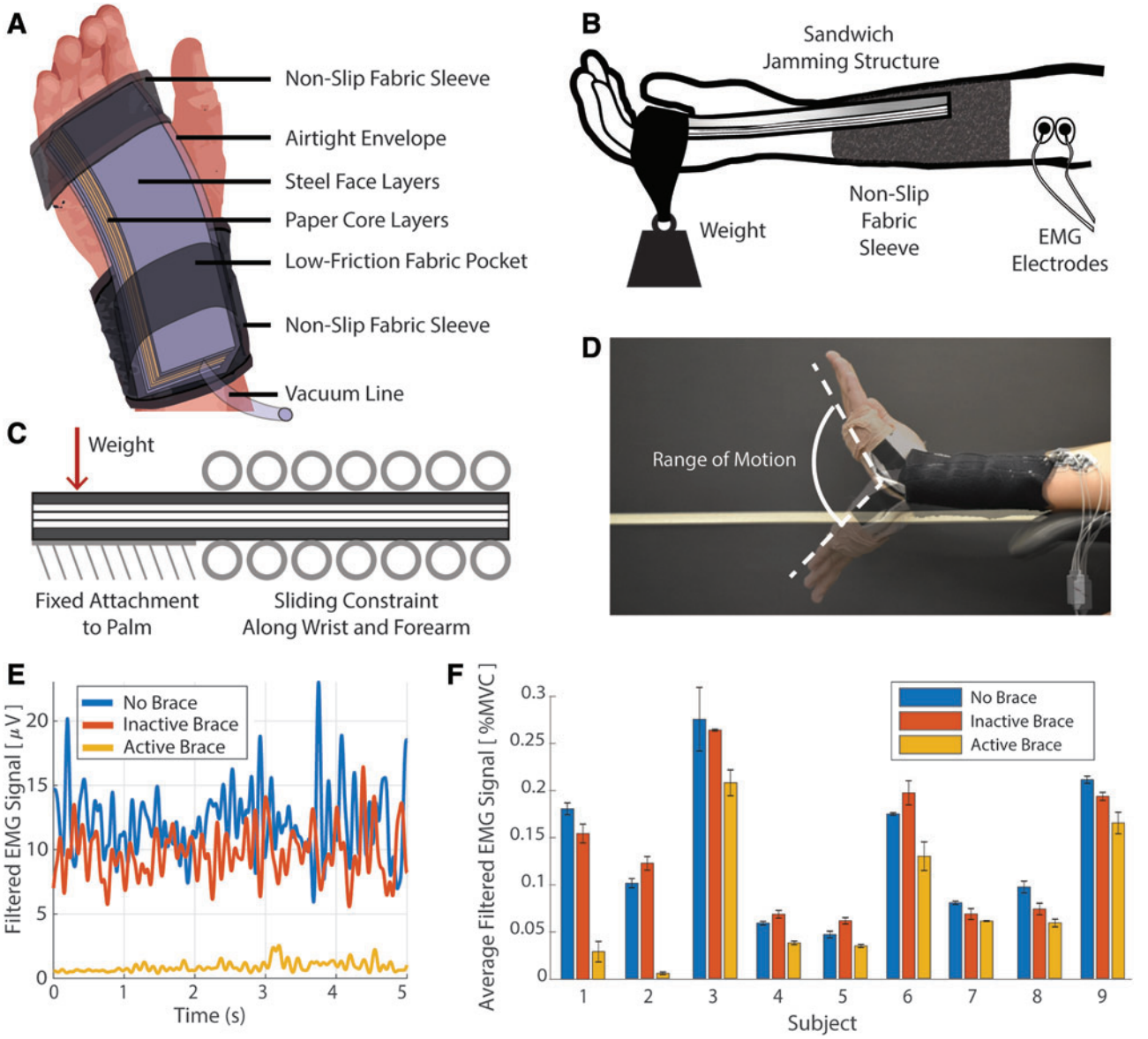

FIG. 6. Overview of the sandwich-jamming wrist orthosis. **(A)** Close-up diagram of orthosis. For simplicity, the hook-and-loop (i.e., Velcro) attachment on the distal fabric sleeve is not shown. **(B)** Diagram of orthosis during isometric hold task. For simplicity, the hook-and-loop attachment and the low-friction fabric constraining the sandwich jamming structure are not depicted. **(C)** Highly simplified free-body diagram of sandwich jamming structure during isometric hold task. Note that during the task, the palm and wrist themselves were free-floating, whereas the forearm was supported by an armrest. **(D)** Range-of-motion trials of a representative human subject in the no-brace and inactive conditions, respectively. Range of motion was largely preserved. **(E)** Time-varying EMG signals for one representative subject during one trial. **(F)** EMG signals for all nine subjects averaged for three trials and normalized with respect to their average EMG signals during maximum voluntary contractions. *Error bars* on the bar plot denote standard error. EMG, electromyography; MVC, maximum voluntary contractions. Color images are available online.

Our study offers four contributions. First, this study proposes the concept of tunable jamming-based sandwich structures, which is one of the first explorations of tunable jamming-based composites in the literature. Previous studies have combined discrete granular and laminar jamming elements,[35] combined discrete granular and fiber-based jamming elements,[14] and integrated sensing and actuation components into jamming structures,[10,36] but did not investigate how to achieve high performance-to-mass, which is a trademark capability of composite materials and structures.

Second, we experimentally showed that our specific implementations of sandwich jamming structures were able to achieve exceptional mechanical properties. The structures outperformed the stiffness-, range-, and yield-to-mass of laminar jamming analogues by one to two orders of magnitude. Furthermore, these sandwich jamming structures well exceeded the performance of other tunable sandwich structures in the literature. Existing tunable sandwich structures have typically been constructed with one of the following features: (1) a core containing electrorheological fluid,[26]

(2) a core containing magnetorheological fluid,[28] (3) a core containing shape-memory material,[27,30] and (4) facesheets that are electrostatically bonded to the core.[29] Among these structures, experimentally validated stiffness ranges are typically well <2, and the highest range found in the literature was 18 (Ref.[29]). Our study experimentally demonstrated that a simple steel-paper sandwich jamming structure could achieve a stiffness range of 1850 in a lightweight form. In contrast to previous embodiments, our structure was low cost, could be rapidly activated, and did not require high voltages that could compromise safe interaction with humans.

As a third contribution, this study provides a theoretical framework for designers to construct and optimize sandwich jamming structures to meet design requirements. Given an existing laminar jamming structure, the improvement ratios and associated contour maps inform designers precisely how the performance metrics of the structure (i.e., stiffness-to-mass, range-to-mass, and yield-to-mass) can be improved by adding a core and adjusting critical design parameters (i.e., thickness ratio, density ratio, elastic modulus ratio, layer number ratio, and friction ratio); these predictions show that improvement ratios of several orders of magnitude may be readily achievable. Moreover, the optimization code and associated contour maps allow designers to select an arbitrary set of face and core materials and rapidly determine the highest performing structure that can meet their mass and volume constraints. Thus, the analysis enables designers to deterministically improve existing structures, as well as design optimal structures from the ground up.

The design example comprises the final contribution of the article, as it provides a feasible solution to a challenging engineering problem. In rehabilitation, previous efforts to determine whether wrist orthoses can reduce muscle activation have been inconclusive, with various studies showing moderately positive,[37] negative,[38] and neutral results.[39] Our study demonstrated that a sandwich-jamming orthosis reduced muscle activation by >40% on a small population of participants, providing a compelling basis for further investigation. Moreover, in contrast to wrist orthoses that have previously been reported, the sandwich-jamming orthosis is highly tunable, allowing significant range of motion and causing no notable increase in muscle activation when inactive.

From a theoretical standpoint, future study will focus on deriving improvement ratios and contour maps for additional advantageous properties of sandwich jamming structures, such as damping, shear stiffness, damping range, and shear stiffness range (all with respect to mass). From an applied perspective, subsequent research will focus on making two design changes that may immediately improve the performance-to-mass of sandwich jamming structures even further: (1) using composite materials (e.g., carbon-fiber-reinforced polymers or fiberglass) as face layers, and (2) increasing the porosity of the core layers (e.g., by laser-cutting honeycomb patterns into the layers). Furthermore, to maximize portability of the sandwich jamming structures while preserving human safety, the sandwich jamming structures will be activated with nonfluidic and nonelectrostatic methods, such as tightening an elastic mesh around the layers.[40] Finally, we will apply our initial efforts to design and model mixed-media jamming structures (e.g., granular-laminar hybrids)[19,41] to create mixed-media sandwich jamming structures with enhanced tunability and conformability. These improvements can augment the mechanical properties and utility of sandwich jamming structures, as well as lay a foundation for their commercial adoption in wearable robots, modern vehicles, and rapidly deployable construction.

Conclusion

This study proposed the novel concept of tunable sandwich-based jamming structures. These structures were experimentally shown to have far higher performance-to-mass ratios than standard laminar jamming structures and existing tunable sandwich structures, as well as obvious versatility advantages over traditional sandwich structures. Theoretical models and finite element simulations were provided that allow designers to deterministically improve the performance-to-mass of laminar jamming structures by converting them to a sandwich architecture. A software routine was presented that also allowed designers to optimize sandwich jamming structures given arbitrary material, mass, and volume constraints. Finally, the utility of sandwich jamming structures was demonstrated through their integration into a wearable robotic device that significantly reduced muscle activation of human subjects in the on state, while having negligible impact on activation in the off state. Overall, sandwich jamming structures were shown to extend the performance boundaries of existing tunable-stiffness mechanisms, setting the stage for ultralight tunable-stiffness devices in the future. Subsequent work will focus on improving performance further through the incorporation of composite materials and portable jamming-activation mechanisms.

Author Disclosure Statement

No competing financial interests exist.

Funding Information

Funding was provided by the National Science Foundation Graduate Research Fellowship award 1122374, the National Science Foundation grant CMMI-1637838, the National Science Foundation grant IIS-1924984, and the Hansjörg Wyss Institute for Biologically Inspired Engineering at Harvard University.

Supplementary Material

Supplementary Data
Supplementary Figure S1
Supplementary Figure S2
Supplementary Figure S3
Supplementary Figure S4
Supplementary Figure S5
Supplementary Figure S6
Supplementary Table S1
Supplementary Table S2
Supplementary Table S3
Supplementary Table S4
Supplementary Table S5

References

1. Vanderborght B, Albu-Schaeffer A, Bicchi A, et al. Variable impedance actuators: a review. Robot Auton Syst 2013;61:1601–1614.

2. Cianchetti M, Ranzani T, Gerboni G, et al. Soft robotics technologies to address shortcomings in today's minimally invasive surgery: the STIFF-FLOP approach. Soft Robot 2014;1:122–131.
3. Manti M, Cacucciolo V, Cianchetti M. Stiffening in soft robotics: a review of the state of the art. IEEE Robot Autom Mag 2016;23:93–106.
4. Narang YS, Vlassak JJ, Howe RD. Mechanically versatile soft machines through laminar jamming. Adv Funct Mater 2018;28:1707136.
5. Amend JR, Brown E, Rodenberg N, et al. A positive pressure universal gripper based on the jamming of granular material. IEEE Trans Robot 2012;28:341–350.
6. Cheng NG, Lobovsky MB, Keating SJ, et al. Design and analysis of a robust, low-cost, highly articulated manipulator enabled by jamming of granular media. In: Proceedings of the IEEE International Conference on Robotics and Automation (ICRA), Saint Paul, MN, May 14–18, 2012, pp. 2922–2927.
7. Kim Y-J, Cheng S, Kim S, et al. A novel layer jamming mechanism with tunable stiffness capability for minimally invasive surgery. IEEE Trans Robot 2013;29: 1031–1042.
8. Kawamura S, Yamamoto T, Ishida D, et al. Development of passive elements with variable mechanical impedance for wearable robots. In: Proceedings of the IEEE International Conference on Robotics and Automation (ICRA), Washington, DC, May 11–15, 2002, pp. 248–253.
9. Follmer S, Leithinger D, Olwal A, et al. Jamming user interfaces: programmable particle stiffness and sensing for malleable and shape-changing devices. In: Proceedings of the 25th Annual ACM Symposium on User Interface Software and Technology, Cambridge, MA, October 7–10, 2012, pp. 519–528.
10. Ou J, Yao L, Tauber D, et al. jamSheets: thin interfaces with tunable stiffness enabled by layer jamming. In: Proceedings of the ACM International Conference on Tangible, Embedded, and Embodied Interactions, Munich, Germany, February 16–19, 2014, pp. 65–72.
11. Stanley AA, Okamura AM. Controllable surface haptics via particle jamming and pneumatics. IEEE Trans Haptics 2015;8:20–30.
12. Zubrycki I, Granosik G. Novel haptic device using jamming principle for providing kinaesthetic feedback in glove-based control interface. J Intell Robot Syst 2017;85:413–429.
13. Jiang A, Xynogalas G, Dasgupta P, et al. Design of a variable stiffness flexible manipulator with composite granular jamming and membrane coupling. In: Proceedings of the IEEE/RSJ International Conference on Intelligent Robots and Systems (IROS), Vilamoura, Portugal, October 7–12, 2012, pp. 2922–2927.
14. Thompson-Bean E, Steiner O, McDaid A. A soft robotic exoskeleton using granular jamming. In: Proceedings of the IEEE International Conference on Advanced Intelligent Mechatronics, Busan, South Korea, July 7–11, 2015, pp. 165–170.
15. Hauser S, Robertson M, Ijspeert A, et al. JammJoint: a variable stiffness device based on granular jamming for joint wearable support. IEEE Robot Autom Lett 2017;2: 849–855.
16. Steltz E, Mozeika A, Rembisz J, et al. Jamming as an enabling technology for soft robotics. In: Proceedings of SPIE 7642, Electroactive Polymer Actuators and Devices (EAPAD), San Diego, CA, April 9, 2010, pp. 1–9.
17. Kuder IK, Arrieta AF, Raither WE, et al. Variable stiffness material and structural concepts for morphing applications. Prog Aerosp Sci 2013;63:33–55.
18. Narang YS, Degirmenci A, Vlassak JJ, et al. Transforming the dynamic response of robotic structures and systems through laminar jamming. IEEE Robot Autom Lett 2018;3: 688–695.
19. Vasios N, Narang YS, Aktas B, et al. Numerical analysis of periodic laminar and fibrous media undergoing a jamming transition. Eur J Mech A Solids 2019;75:322–329.
20. Bureau M, Keller T, Perry J, et al. Variable stiffness structure for limb attachment. IEEE Int Conf Rehabil Robot 2011;2011:5975350.
21. Simon T, Thomas B, Smith R. Low-profile jamming technology for medical rehabilitation. IT Prof 2015;17: 28–34.
22. Browning RC, Modica JR, Kram R, et al. The effects of adding mass to the legs on the energetics and biomechanics of walking. Med Sci Sports Exerc 2007;39:515–525.
23. Watson JC, Payne RC, Chamberlain AT, et al. The energetic costs of load-carrying and the evolution of bipedalism. J Hum Evol 2008;54:675–683.
24. Anderson JD. Fundamentals of Aerodynamics, 5th ed. New York: McGraw-Hill, 2010.
25. Zenkert D. Handbook of Sandwich Construction. Cradley Heath, UK: Engineering Materials Advisory Services, Ltd., 1997.
26. Gandhi MV, Thompson BS, Choi SB. A new generation of innovative ultra-advanced intelligent composite materials featuring electro-rheological fluids: an experimental investigation. J Compos Mater 1989;23:1232–1255.
27. Birman V. Stability of functionally graded shape memory alloy sandwich panels. Smart Mater Struct 1997; 6:278.
28. Yalcintas M, Dai H. Magnetorheological and electrorheological materials in adaptive structures and their performance comparison. Smart Mater Struct 1999;8:560.
29. Bergamini A, Christen R, Maag B, et al. A sandwich beam with electrostatically tunable bending stiffness. Smart Mater Struct 2006;15:678.
30. Butaud P, Foltte E, Ouisse M. Sandwich structures with tunable damping properties: on the use of shape memory polymer as viscoelastic core. Compos Struct 2016;153: 401–408.
31. Zenkert D. Introduction to Sandwich Construction. Cradley Heath, UK: Engineering Materials Advisory Services, Ltd., 1995.
32. Bauchau OA, Craig JI. Structural Analysis with Applications to Aerospace Structures. New York: Springer, 2009.
33. Plantema FJ. Sandwich Construction. New York: John Wiley & Sons, 1966.
34. Allen HG. Analysis and Design of Structural Sandwich Panels. Oxford, UK: Pergamon Press, 1969.
35. Langer M, Amanov E, Burgner-Kahrs J. Stiffening sheaths for continuum robots. Soft Robot 2018;5:219–303.
36. Yao L, Niiyama R, Ou J, et al. PneUI: Pneumatically actuated soft composite materials for shape changing interfaces. In: Proceedings of the Annual ACM Symposium on User Interface Software and Technology, New York, NY, October 2013, pp. 13–22.
37. Jansen CWS, Olson S, Hasson SM. The effect of use of a wrist orthosis during functional activities on surface

electromyography of the wrist extensors in normal subjects. J Hand Ther 1997;10:283–289.
38. Bulthaup S, Cipriani DJ, Thomas JJ. An electromyography study of wrist extension orthoses and upper extremity function. Am J Occup Ther 1999;53:434–440.
39. Johansson L, Bjring G, Hgg GM. The effect of wrist orthoses on forearm muscle activity. Appl Ergon 2004;35: 129–136.
40. Santiago JLC, Godage IS, Gonthina P, et al. Soft robots and kangaroo tails: modulating compliance in continuum structures through mechanical layer jamming. Soft Robot 2016;3:54–63.
41. Narang YS. Achieving Mechanical Versatility in Robots and Structures Through Laminar Jamming. PhD thesis, Harvard University, 2018. Chapter 5.

Address correspondence to:
Robert D. Howe
Paulson School of Engineering and Applied Sciences
Harvard University
Cambridge, MA 02138
USA

E-mail: howe@seas.harvard.edu